Non-centrosymmetry Effects and Polarity Determination in III–V Semiconductors

Knut Marthinsen,[a]* Thomas Lindheim[b] and Ragnvald Høier[b]

[a]*SINTEF Materials Technology, N-7034 Trondheim, Norway, and [b]Department of Physics, Norwegian University of Science and Technology, NTNU, N-7034 Trondheim, Norway. E-mail: knut.marthinsen@matek.sintef.no*

Abstract

A method for determining polarity in III–V semiconductors is discussed. It is based on comparison of two conjugate four-beam CBED patterns tilted away from the [011] zone axis. The method was originally developed for GaAs, but it is shown that with carefully chosen diffraction conditions strong effects of non-centrosymmetry may be observed for III–V semiconductors in general. The polarity can be uniquely determined from observed intensity differences in the ±200 discs. Examples from GaAs and InP are given. The general conditions for strong asymmetry effects in the ±200 discs are that the structure-factor magnitudes of the reflections involved are about of the same size and that the three-phase invariants involved are as close as possible to ±π/2. The asymmetry effect is rather insensitive to thickness but weakens as the thickness approaches the extinction lengths of the weak reflections involved. It is shown that U_{200} for GaAs (sensitive to bonding) in principle may be determined from the gap between the black lines in one of the 200 discs if the other parameters can be controlled. It is further suggested that the Al content x in $Al_xGa_{1-x}As$, on which U_{200} is strongly dependent, can be determined from this gap when $x < 0.3$–0.4.

1. Introduction

An important aspect of the characterization of semiconductors with a non-centrosymmetric structure is the determination of absolute polarity of the specimen. However, this is not always straightforward and depends in general on carefully chosen diffraction conditions. Several electron diffraction methods have been proposed for the determination of polarity in non-centrosymmetric crystals (*e.g.* Taftø & Spence, 1982; McKernan & Carter, 1990; Spellward & James, 1991). In the work of Taftø & Spence (1982), a very simple method for polarity determination was proposed that may be used for crystals of the sphalerite structure. It is based on comparing the intensity in the ±200 convergent-beam electron diffraction (CBED) discs for two conjugate four-beam cases tilted away from the [011] zone axis. For GaAs, it has been shown that very large asymmetry effects can be obtained even though GaAs deviates very little from

centrosymmetry. These strong asymmetry effects can be explained qualitatively based on quasi-kinematical arguments making use of the polynomial expression of Cowley & Moodie (1962) with all excitation errors set to zero (Taftø & Spence, 1982; Ishizuka & Taftø, 1984).

In the present work, we have reinvestigated and discussed the method of Taftø & Spence within the framework of the Bloch-wave theory and dynamical many-beam calculations. However, for the sake of completeness, the qualitative interpretations made in the previous works are also included. The aim of the present work has been to evaluate the general applicability of the method and to see if it is possible to establish some general conditions when strong asymmetry effects may be observed. The fact that such large effects are produced for GaAs where the deviation from centrosymmetry is so small makes this effect very intriguing, and suggests that it can be used for quantitative purposes. The object has therefore further been to evaluate the potential that the strong asymmetry effects observed in GaAs has for quantitative purposes. Some preliminary results from this work have been published previously (Marthinsen & Høier, 1992).

2. The asymmetry effect in GaAs and its qualitative interpretation

Fig. 1 shows a four-beam simulation of the ±200 asymmetry effect in GaAs corresponding to the original experiment by Taftø & Spence (1982). With respect to the [011] zone axis, the incident-beam direction corresponds to a tilt of about 13° around the (100) direction such that the Bragg condition is fulfilled for the 200, $\bar{9}1\bar{1}$ and $11,1,\bar{1}$ reflections in Fig. 1(a), and for the reflectons $\bar{2}00$, $\overline{11},1,\bar{1}$ and $91\bar{1}$ in Fig. 1(b). Schematic drawings showing the reflections involved and corresponding scattering paths in the respective (conjugate) cases are given below for each case. The crossing lines in the discs, which are a consequence of scattering from the direct beam *via* the 911- and 11,1,1-type reflections, appear black in the $\bar{2}00$ disc and white in the 200 disc suggesting destructive and constructive interference, respectively. Although GaAs has a very small deviation from centrosymmetry (Ga and As have atomic number $Z = 31$ and 33, respectively), the difference between these two conjugate cases is striking.
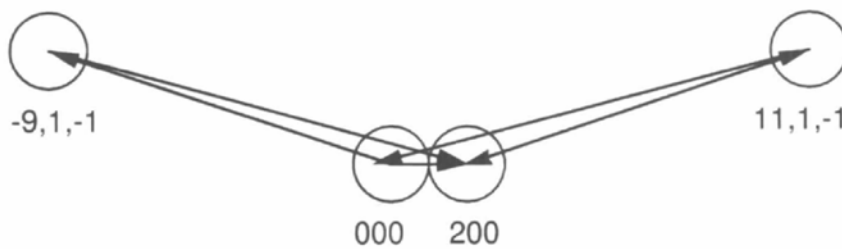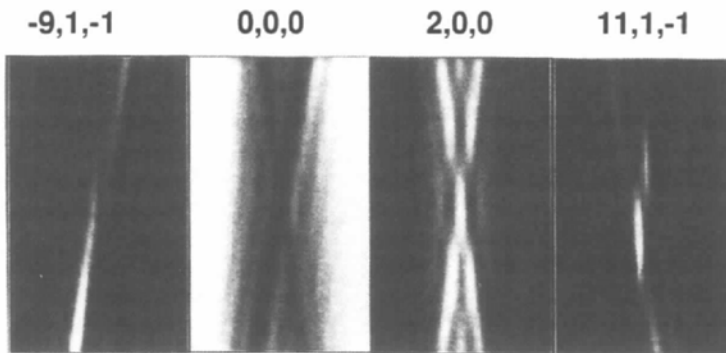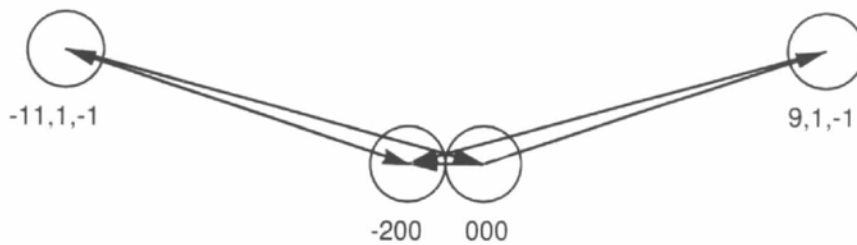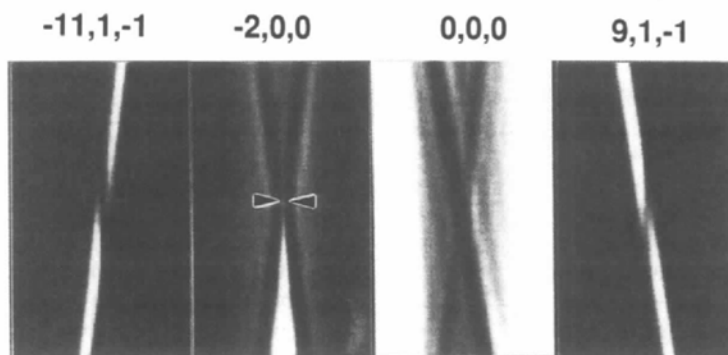
Fig. 1. Calculated four-beam CBED intensity distributions. (a) 200 case and (b) conjugate $\bar{2}$00 case. Position of gap between intersecing lines in the $\bar{2}$00 disc are indicated. Schematics indicating scattering paths are shown below each case.

The simulations in Fig. 1, as well as all the computer simulations in the present work, were carried out with a standard Bloch-wave simulation program (Zuo, Gjønnes & Spence, 1989). For simplicity and since the present work is focused on qualitative interpretations, only three and four beams are included in the calculations. The structure factors (elastic part) are based on tabulated scattering factors from Doyle & Turner (1968). Absorption is included in the simulations using the subroutine *ATOM* (Bird & King, 1990), however, the structure-factor phases used in the discussion refer to the elastic part of the structure factor. The Debye–Waller factors used for GaAs were $B_{Ga} = 0.637$ and $B_{As} = 0.686$ Å^2 (at 300 K). The corresponding values for InP were $B_{In} = 0.333$ and $B_{P} = 0.270$ Å^2. If not otherwise stated, the simulations have been carried out for 100 keV electrons and with a specimen thickness of 2000 Å. As illustrated in Fig. 2, the GaAs (InP) unit cell is defined with Ga (In) at $(0, 0, 0)$ and As (P) at $(\frac{1}{4}, \frac{1}{4}, \frac{1}{4})$.

Following Ishizuka & Taftø (1984), the ±200 asymmetry effect in Fig. 1 can be explained qualitatively making use of Cowley's polynomial expression for dynamical diffraction with all excitation errors put equal to zero. The structure factors of the reflections considered are so small that all extinction lengths are more than 4000 Å at 100 keV (*cf.* Table 1). Therefore, phase changes due to change in thickness can be neglected up to about 1000 Å for such weak reflections. For thicknesses much lower than actual extinction lengths, the phase of a scattering path is the sum of the phase change of $-\pi/2$ associated with each scattering process and φ_i for each structure factor involved. The total phase change φ for n times multiple scattering can then be written

$$\varphi = \sum_{i=1}^{n} -\pi/2 + \varphi_i. \quad (1)$$

Since the atoms are almost identical, we may write the atomic form factors as $f_{Ga} = \bar{f} - \Delta f$ and $f_{As} = \bar{f} + \Delta f$, where $\bar{f}$ is the mean value and Δf is defined positive. The unit cell is defined with Ga and As atoms at $(0, 0, 0)$ and
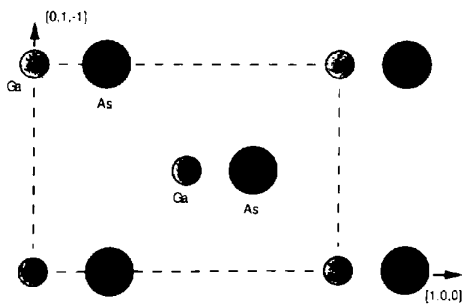

Fig. 2. The GaAs unit cell in the [011] projection. The absolute physical orientation of the crystal is consistent with the diffraction pattern in Fig. 1.

$(\frac{1}{4}, \frac{1}{4}, \frac{1}{4})$, respectively, and in the equivalent positions of the f.c.c. structure. To first order of Δf in the amplitude and neglecting Δf in the phases, the structure factor then becomes

$$F_{hkl} = \begin{cases} 0 & \text{mixed indices} \\ 4 \times 2^{1/2} \bar{f} \exp(\pm i\pi/4) & h + k + l = 4n \pm 1 \\ -8\Delta f & h + k + l = 4n + 2 \\ -8\bar{f} & h + k + l = 4n. \end{cases}$$
$$(2)$$

Neglecting the coupling between the two odd-index reflections with reciprocal vector $[20, 0, 0]$, $(U_{20, 0, 0}/U_{200} = 1/9)$, each four-beam case may approximately be considered as a superposition of two three-beam cases. This is strictly not correct (*e.g.* a three-beam case does not generally decompose into two independent two-beam cases if the coupling is neglected), however, in this case, the assumption is supported by simulations with $U_{20, 0, 0} = 0$, which show no visual change in the diffraction pattern. Then there are essentially two scattering paths into the 200-type reflections. One is the direct path

$$(000) \rightarrow (\pm 200) \Rightarrow \varphi = -\pi/2 + \pi = +\pi/2 \quad (3)$$

and the other one is *via* the odd-index reflections that are of the type $4n + 1$ and $4n - 1$ for the $\bar{2}00$ and 200 cases, respectively, *i.e.*

$$(000) \rightarrow (4n + 1) \rightarrow (\bar{2}00) \Rightarrow$$
$$\varphi = (-\pi/2 + \pi/4) + (-\pi/2 + \pi/4) = -\pi/2$$
$$(000) \rightarrow (4n - 1) \rightarrow (200) \Rightarrow$$
$$\varphi = (-\pi/2 - \pi/4) + (-\pi/2 - \pi/4) \doteq +\pi/2.$$
$$(4)$$

Hence, the direct scattering into the $\bar{2}00$ reflection is π out of phase with the scattering over each of the two other paths giving destructive interference, while both the double-scattering paths scatter in phase with the direct path into 200 giving constructive interference. All scattering paths are of approximate equal strength. This explains the black and white crosses observed in the ±200 discs in GaAs.

If we, on the other hand, consider Ge, which is in between Ga and As in the periodic system, Ge has diamond structure and is centrosymmetric. In this case, $\Delta f = 0$ and the 200 reflections are extinguished and the direct path is no longer existent. As a consequence, there is constructive interference in both conjugate cases and only a white cross appears in both cases.

3. Polarity determination in GaAs

The above results for GaAs can be utilized to determine the polarity of the crystal, *i.e.* the absolute chemical

Table 1. *Selected structure factors and corresponding extinction lengths in GaAs calculated at 100 keV*

'Total' is the elastic part plus the absorptive part of the structure factor.

Reflection	Elastic		Total		
	$|U_g|$ (Å^{-2})	φ_g (°)	$|U_g|$ (Å^{-2})	φ_g (°)	ζ_g (Å)
± 200	0.003807	0.0	0.003816	-3.85	7079
$11,1,\bar{1}$	0.003734	-44.81	0.003834	-55.82	7047
$\overline{11},1,\bar{1}$	0.003734	44.81	0.003775	33.62	7157
$\bar{9}1\bar{1}$	0.006261	-44.76	0.006411	-54.70	4214
$91\bar{1}$	0.006261	44.76	0.006305	34.64	4285

orientation of a specimen. In order to distinguish non-equivalent directions such as [100] and [$\bar{1}$00], three directions need to be specified: the sense of the basis and two indexed reflections. Two may be chosen freely and the third then determines the polarity consistent with the choices made (Spellward & James, 1991). If strong absorption effects are present, the phase differences for conjugate reflections shown in Table 1 will in principle appear as intensity differences between conjugate discs even in the two-beam case (Bird, 1990) and the polarity can in principle be determined. However, this is a second-order effect and polarity determination has in general to be based on dynamical many-beam interactions, which in practice are present in all electron diffraction experiments. The polarity determination is then based on a comparison of the intensity in the **g** and $-$**g** discs for two diffraction conditions differing only by a change of **g** in the incident-beam direction **K**. Non-centrosymmetry will in general introduce a loss of translation symmetry between the **g** and $-$**g** discs, even when only reflections in the ZOLZ are exited. The reason for this is interchanging elements in the eigenvectors (*e.g.* Marthinsen, 1993). This is exactly the diffraction conditions we have for GaAs in Fig. 1, and the intensity differences observed between the ± 200 reflections are an extreme example of this loss of translational symmetry. The position of the white cross relative to the black one determines uniquely the polarity of a GaAs sample. With the definition of basis given above, the observations in Fig. 1 are consistent with an absolute orientation of the crystal relative to the diffraction pattern in Fig. 1 as shown in Fig. 2. A white cross in the disc to the right of the direct beam implies that As lies to the right of Ga in the specimen and *vice versa* if the white cross is to the left.

4. Dynamical Bloch-wave theory

Within dynamical Bloch-wave theory, the intensity in a CBED disc **g**, neglecting absorption, is given by the following intensity expression (*e.g.* Spence & Zuo, 1992):

$$I_g(t) = \sum_i |C_0^{i*} C_g^i|^2 + 2\sum_{i>j}\sum |C_0^{i*} C_g^i C_0^j C_g^{j*}|$$
$$\times \cos[(\gamma^i - \gamma^j)t + \alpha^{ij}]. \quad (5)$$

Here, γ^i and C_g^i are Bloch-wave eigenvalues and Bloch-wave eigenvector components, respectively. α^{ij} is the phase of $C_0^{i*} C_g^i C_0^j C_g^{j*}$.

The two conjugate four-beam cases we are discussing will have the same eigenvalues but a conjugated eigenvector set (neglecting absorption), which reverses the sign of α^{ij}. This change of sign is thus the origin of the asymmetry observed between the 200 and $\overline{200}$ discs (Marthinsen, 1993). For the special case of a centrosymmetric crystal, the eigenvectors (again neglecting absorption) will be real, $\alpha^{ij} = 0$, and the asymmetry obtained for non-centrosymmetric crystals disappears. In the non-centrosymmetric case, the size of the phase term α^{ij} depends on the magnitude of the individual structure factors, $U_g = |U_g| \exp(i\varphi_g)$ and the three-phase structure invariants involved, $\Psi_g = \varphi_{-g} + \varphi_h + \varphi_{g-h}$, respectively.

Many-beam effects are in many cases conveniently discussed in terms of a perturbed two-beam case, incorporating the effects of all reflections apart from the two strongest, say **0** and **g**, through an effective potential U_g^{eff} by using a perturbation series (Bethe, 1928). In this case, the standard two-beam intensity expression becomes (Zuo, Høier & Spence, 1989)

$$I_g = [|U_g^{\text{eff}}|^2/(K\Delta\gamma)^2] \sin^2(\pi t \Delta\gamma), \quad (6)$$

where $\Delta\gamma$ is the difference between the roots of the modified dispersion equation. In the three-beam case with only one weak beam **h**, the effective structure factor is given by

$$|U_g^{\text{eff}}|^2 = |U_g|^2[1 - (|U_h||U_{g-h}|/|U_g|2Ks_h)\cos\Psi$$
$$+ (|U_h||U_{g-h}|/|U_g|2Ks_h)^2]. \quad (7)$$

5. Simulations and discussion

5.1. *Structure-factor amplitude and phase sensitivity*

As mentioned above, the two conjugate four-beam cases we are discussing can be discussed in terms of two superimposed nearly equivalent three-beam interactions, *i.e.* 000, 200, $11,1,\bar{1}$ and 000, 200, $\bar{9}1\bar{1}$ and the conjugate cases, respectively, since the coupling between the odd-index reflections, *i.e.* $20,0,0$, may be neglected. The magnitude of the structure factors involved are approximately equal (*cf.* Table 1) and the three-phase structure

invariants involved have values $-89.6°$ in the 200 case and $+89.6°$ in the $\bar{2}00$ case, respectively.

Figs. 3(b) and (c) illustrate the effect of increasing the magnitude of the structure factor U_{200} by a factor of 5 and 10, respectively. It is seen that the asymmetry weakens and completely disappears when $|U_{200}|$ gets large as compared with the other reflections involved. This may be understood by the fact that when $|U_{200}|$ increases it will be less affected by the other reflections involved, cf. (7). The ± 200 reflections will become more and more symmetric as they would be in a pure two-beam situation.

In Figs. 4(b) and (c), the phase φ_{200} (for the elastic part, originally equal to $0°$) is gradually changed so that the three-phase invariants in each case approach 0 and $180°$ (or π), respectively. To make the three-phase invariant equal $180°$, φ_{200} is changed by $90°$. The direct-scattering path then comes out of phase with the scattering via the odd-index reflections in both the conjugate cases and thereby causing destructive interfer-

ence. Again, it is seen that the asymmetry disappears. 0 and π are the only values the three-phase invariants can adopt in a centrosymmetric crystal, e.g. for Ge. This is almost exactly the value in Fig. 4(c) and the asymmetry correspondingly disappears.

5.2. Asymmetry effects in InP

The above simulations indicate that in order to observe asymmetry the three-phase invariant should be as close as possible to its non-centrosymmetric values $\pm 90°$ ($\pm \pi / 2$) and the reflections involved should be of equal strength. Like GaAs, InP also has the sphalerite structure. However, although InP is far more acentric, it does not show the same strong asymmetry effects under the same diffraction conditions. The three-phase invariant is about $45°$, but the 200 reflection is almost four times larger than the odd-index reflections. By tilting the incident beam in the $[0\bar{1}1]$ direction, the Laue circle gets smaller and the excited reflections move
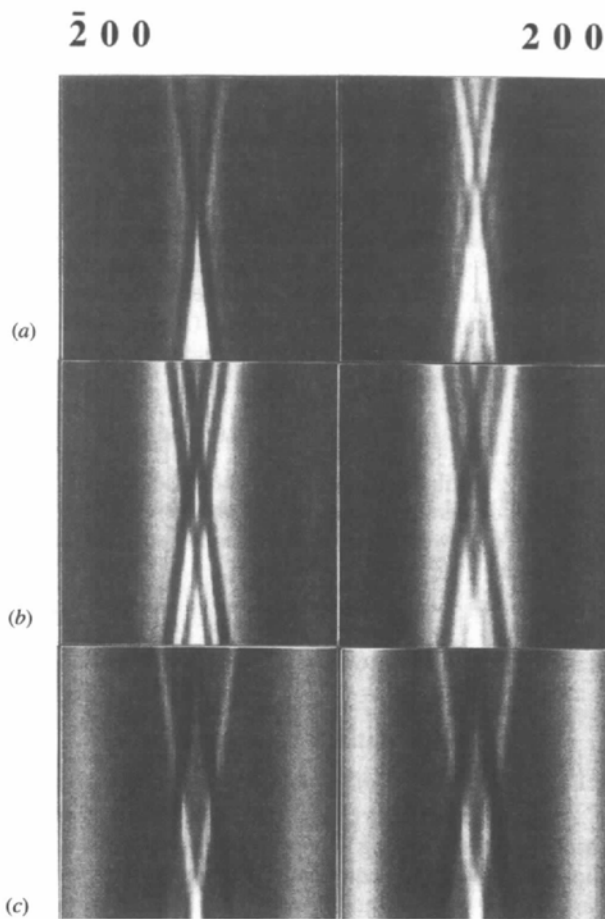

Fig. 3. Calculations for ± 200 discs for modified structure-factor amplitudes. 100 keV, 2000 Å. True pattern included for comparison. (a) Unmodified structure factors, (b) $|U_{200}| \times 5$, and (c) $|U_{200}| \times 10$.
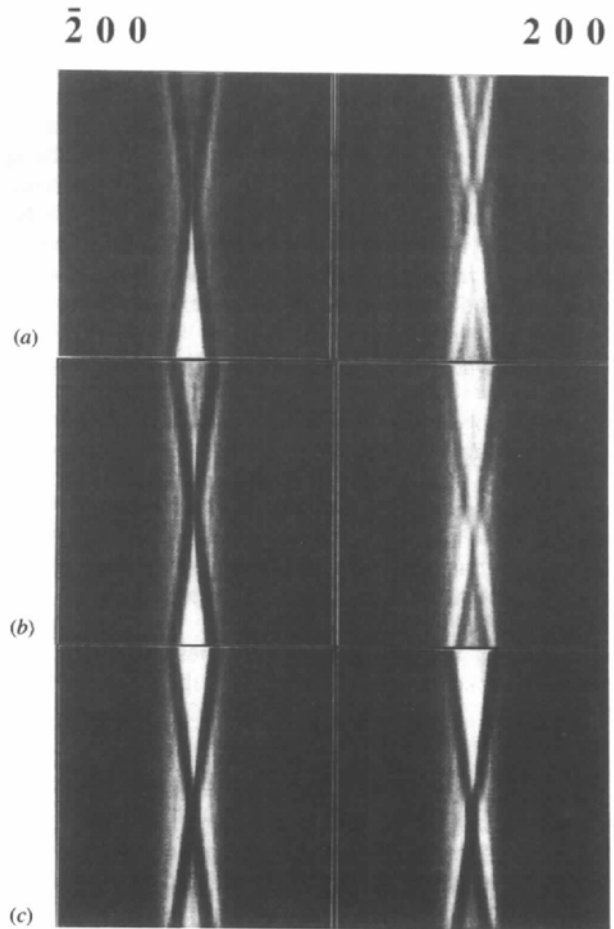
Fig. 4. Calculations for ± 200 discs for modified structure-factor phases. 100 keV, 2000 Å. True pattern included for comparison. (a) Unmodified structure factors, $\Psi \simeq \mp 90°$, (b) $\Psi \simeq -135$, $+45°$, and (c) $\Psi \simeq -180$, $0°$.

inward along the systematic odd-index row $(2n+1,1,\bar{1})$ in Fig. 1. Along this row, the reflections become stronger as n decreases. The phases are almost constant but change sign for every second reflection. Table 2 shows the various diffraction conditions, structure-factor magnitudes and three-phase invariants in the 200 case for InP. The calculated 200 and conjugate $\bar{2}00$ discs are given in Fig. 5. It is seen that when the structure factors again approach the same order of magnitude the distinct asymmetry gradually reappears. For the cases in Fig. 5, all extinction lengths are less than 1600 Å, which suggest that it is possible to observe asymmetry even though the interacting beams are not weak.

5.3. Thickness sensitivity

We now return to GaAs. As already mentioned, all extinction lengths involved are large and the observed effect should be relatively thickness independent. In Fig. 6, the two conjugate cases are simulated for a wide range of specimen thicknesses and we see that this is actually the case. A clear asymmetry is present for thicknesses up to 3000 Å where the double scattering becomes dominant and the asymmetry is almost wiped out. Notice that the position of the lines in the $\bar{2}00$ discs seems to be constant and independent of thickness. The conservation of the asymmetry for both GaAs and InP for relatively large specimen thicknesses (compared with the largest extinction distance involved) may possibly be related to the large asymmetries in the the phases of the total structure factors (right columns in Table 1, which include the absorptive part of the potential).

Table 2. *Comparing conditions for various diffraction cases in InP for the 200 and the two odd-index reflections*

Diffraction case	Odd-index reflections involved	Three-phase invariant (°)	$|U_{odd\ index}|_{max}$ (Å^{-2})
(a)	$11,1,\bar{1}$ and $\bar{9}1\bar{1}$	−48.2	0.0057
(b)	$91\bar{1}$ and $\bar{7}1\bar{1}$	+44.2	0.0100
(c)	$71\bar{1}$ and $\bar{5}1\bar{1}$	−42.3	0.0178
(d)	$51\bar{1}$ and $\bar{3}1\bar{1}$	+45.4	0.0323
$|U_{200}|$			0.0220

5.4. 200 intensity gap in GaAs

The minimum distance, *i.e.* the gap in Fig. 1 (indicated by arrows), between the lines in the $\bar{2}00$ disc appears to be independent of specimen thickness. However, the gap is believed to be dependent on the 200 structure factor (Ishizuka & Taftø, 1984). Since $|U_{200}|$ is proportional to the difference Δf of the atomic form factors of Ga and As, it is very sensitive to the charge transfer between these two atoms, and thus to bonding. With this motivation, the properties of the gap were examined more closely.

Fig. 7 shows simulations of the $\bar{2}00$ discs in each of the separate three-beam cases in the decoupled four-beam $\bar{2}00$ case, *i.e.* the 000, $\bar{2}00$ $\overline{11},1,\bar{1}$ (Fig. 7a) and the 000, $\bar{2}00$, $91\bar{1}$ (Fig. 7b) case, respectively. A straight black line in the $\bar{2}00$ disc without any splitting is obtained in both cases. The absence of the gap or signs of it in these simulations seems to imply that the gap is a genuine four-beam effect and thus of a different
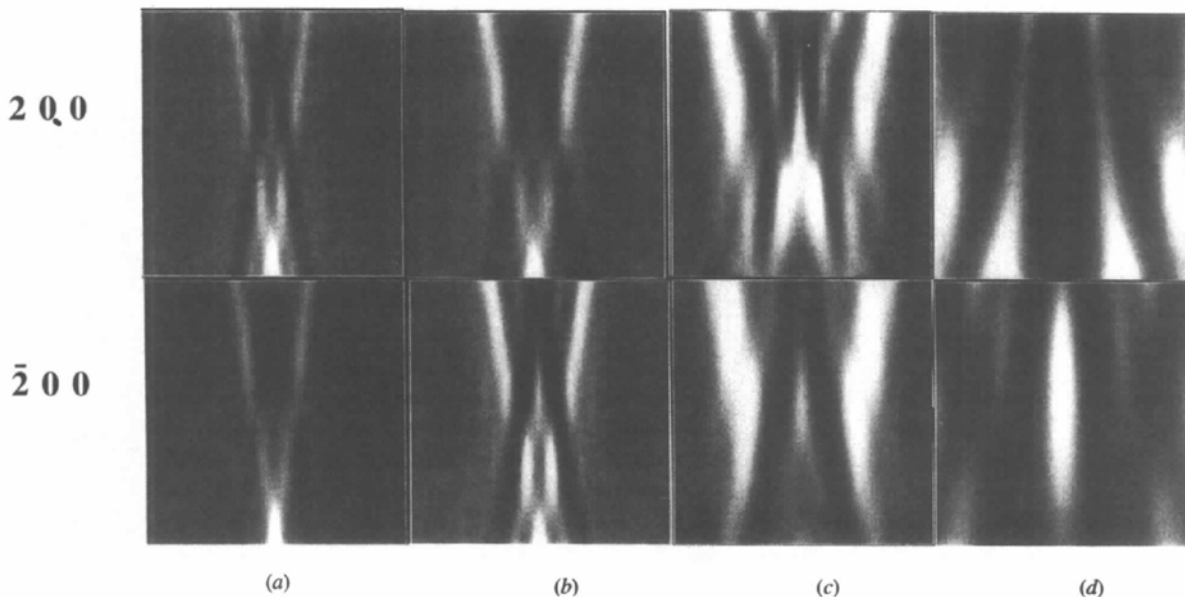

Fig. 5. Calculations for InP. 200 disc at the top and $\bar{2}00$ at the bottom. The respective diffraction cases correspond to the ones given in Table 2 and involve the following odd-index reflections: (a) $11,1,\bar{1}$ and $\bar{9}1\bar{1}$; (b) $91\bar{1}$ and $\bar{7}1\bar{1}$; (c) $71\bar{1}$ and $\bar{5}1\bar{1}$; and (d) $51\bar{1}$ and $\bar{3}1\bar{1}$ and conjugate reflections.

character from the three-beam gaps discussed by *e.g.* Zuo, Gjønnes & Spence (1989), Zuo, Høier & Spence (1989) and Høier, Bakken, Marthinsen & Holmestad (1993). In that case, the gap is directly proportional to the coupling structure factor. The case presented here has almost equal scattering strengths among different paths and involves four different beams. A simple explanation of the present four-beam effect (gap), however, can be given within the 'phase addition' approach. Each of the two double-scattering paths *via* the odd-index reflections interfere destructively with the $\bar{2}00$ reflection but, close to and at the four-beam condition where the two double-scattering paths act together, we get constructive interference. The same argument also gives high intensity at the four-beam position in the 200 disc.

Line scans, or rocking curves, across the 200 disc through the Bragg position in the [100] direction are given in Fig. 8 for several specimen thicknesses. The gap width (defined as the distance between the two first side minima) is seen to be only weakly dependent on the thickness between 1200 and 2000 Å. The intensity of the central maxima increases with increasing thickness while the side maxima intensity decreases. This is so because the double scattering, which dominates close to the Bragg position, becomes relatively stronger than the single scattering for increasing thickness (Ishizuka & Taftø, 1984). It follows also that the 200 structure factor, governing the single scattering, is most sensitive to the intensity of the side maxima as exemplified in Fig. 9. This figure shows rocking curves for the $\bar{2}00$ disc with varying 200 structure-factor magnitude. Increasing

$|U_{200}|$ increases the side maxima and only slightly decreases the central peak. The gap distance reflects the balance between the single and double scattering and decreases with increasing $|U_{200}|$.

However, the gap also depends on the other structure factors involved. Three parameters influencing the gap width are summarized in Fig. 10. For small and moderate deviations from their initial values, the gap width is proportional to $|U_{\bar{9}1\bar{1}}|$ and inversely proportional to $|U_{200}|$. If it is assumed that the gap is proportional to the effective potential $|U_{200}^{\text{eff}}|$, these variations can be understood qualitatively from the effective potential expression in (7) with the $\cos(\Psi)$ terms put equal to zero (which is a good approximation in this case). In the 200 three-beam case (as discussed previously, considering the four-beam case as a superposition of two three-beam cases), $|U_{\bar{9}1\bar{1}}|$ represents the coupling and appears in the numerator of the correction term in (7), while $|U_{200}|$ appears in the denominator, *i.e.* $|U_{200}^{\text{eff}}|$, and thus the gap increases with $|U_{\bar{9}1\bar{1}}|$ and decreases with $|U_{200}|$, in accordance with the observations in Fig. 10 for small and moderate deviations from their original values. For larger deviations, by a factor of two or more, the response to a change in the structure-factor magnitudes reverses. The reason for this behaviour is more complex and the simple perturbed two-beam-approach arguments given above are no longer valid. In addition to the structure factors involved, the gap width is also seen to be dependent on thickness. Fig. 10 illustrates an involved dependence of the different parameters, so unless some of them are known or may be controlled, it may be difficult to extract
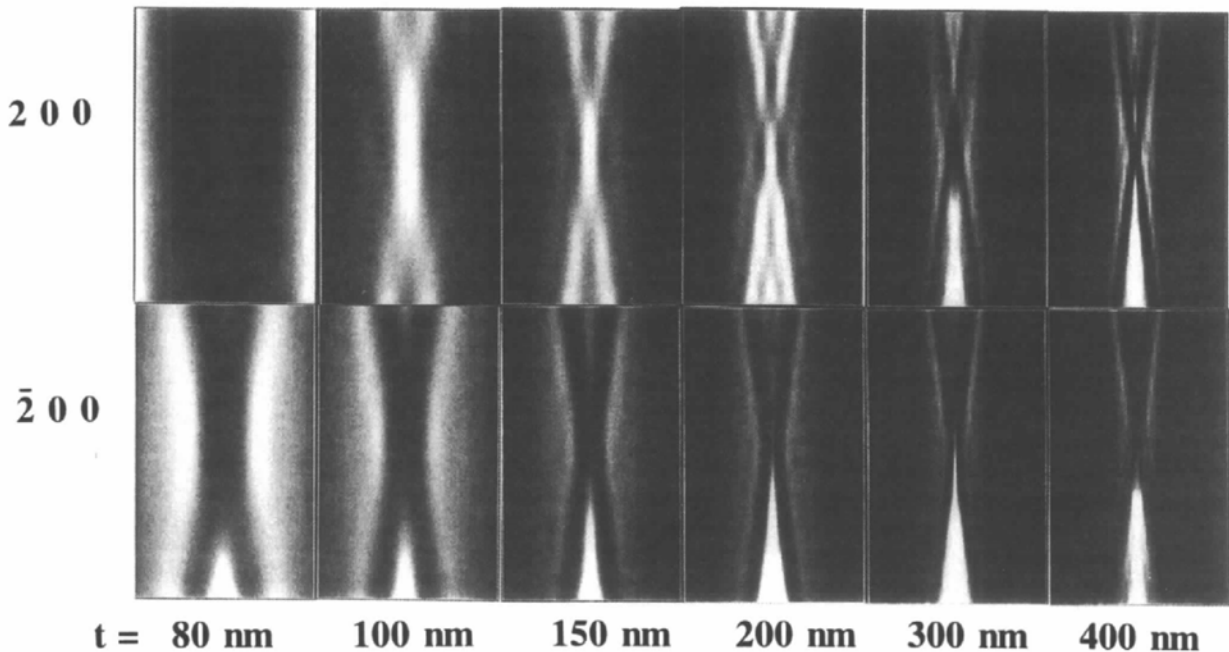

Fig. 6. Specimen-thickness dependence for the $\bar{2}00$ and the conjugate 200 disc for GaAs. 100 keV.

one parameter, independently of the others, from the gap width alone.

5.5. *Determination of Al content in Al$_x$Ga$_{1-x}$As*

As a particular example to see if the 200 gap still may be used for quantitative purposes, we have briefly looked at the possibility of determining the Al content in Al$_x$Ga$_{1-x}$As. This is based on the fact that $|U_{200}|$ will increase with increasing x, *i.e.* an increasing amount of Al. This may be seen from the structure-factor expression for $h + k + l = \pm 2n$ reflections:

$$U_{200} \propto 4[xf_{Al} + (1-x)f_{Ga} - f_{As}]$$
$$= 4[x(f_{Al} - f_{Ga}) + (f_{Ga} - f_{As})]. \quad (8)$$

The idea is then that, if we can determine U_{200} very accurately, x can also be determined quite accurately.

Several methods for the determination of the Al content in Al$_x$Ga$_{1-x}$As with electron diffraction have been proposed (*e.g.* Kakibayashi & Nagata, 1986; Eaglesham & Humphreys, 1986; Stobbs *et al.*, 1989). The advantage of using electron diffraction for this purpose is that very small areas (down to some tens of ångströms with CBED) can be investigated. This means for instance that one can investigate individual layers in semiconductor heterostructures. However, a problem with the methods that have been proposed earlier is the accuracy, typically of the order of 3–5%, which in special cases is not as good as required.

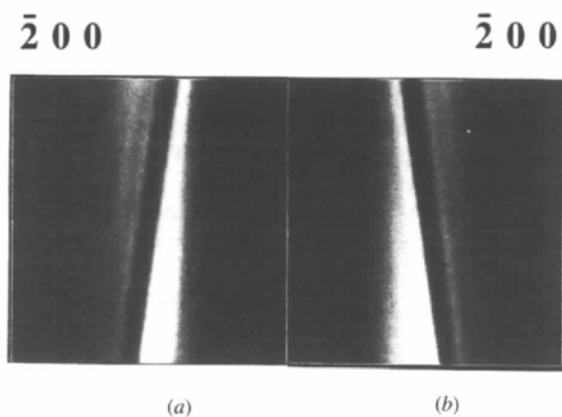$\bar{2}\,0\,0$ $\bar{2}\,0\,0$

(a)   (b)

Fig. 7. Three-beam calculations of the $\bar{2}00$ disc intensities in GaAs. 100 keV, 2000 Å. (*a*) $\bar{2}00$ disc resulting from coupling to the odd-index reflection $\overline{11},1,\bar{1}$. (*b*) $\bar{2}00$ disc resulting from coupling to the reflection $\bar{9}1\bar{1}$.
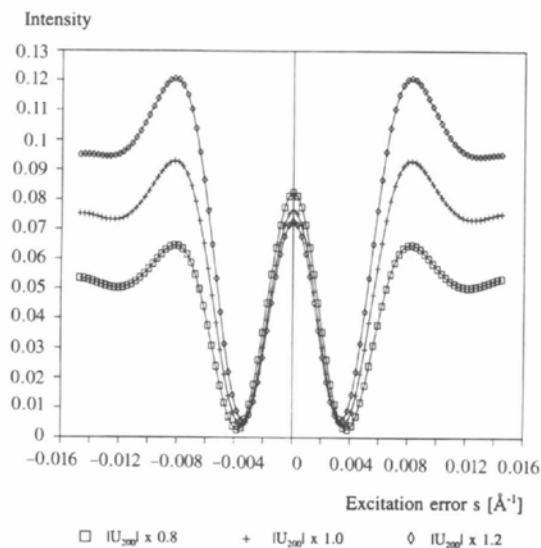

Fig. 9. Rocking curves for the $\bar{2}00$ reflection as a function of $|U_{200}|$.

☐ $|U_{200}| \times 0.8$ + $|U_{200}| \times 1.0$ ◊ $|U_{200}| \times 1.2$

Fig. 8. Simulated rocking curves for the $\bar{2}00$ reflection with different specimen thicknesses.

☐ 1000 Å   + 1200 Å   ◊ 1500 Å   ▲ 2000 Å   × 3000 Å
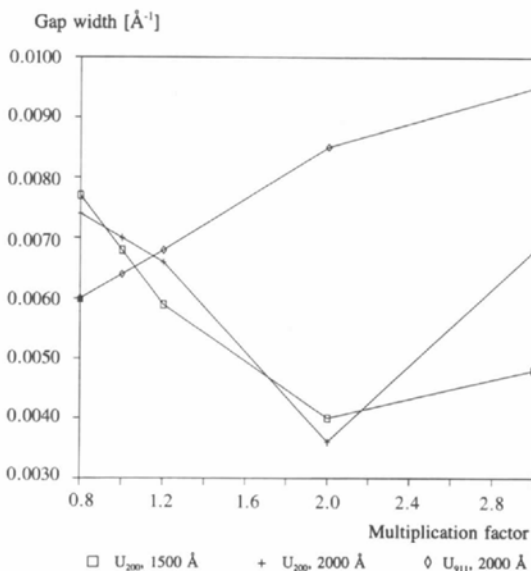
Fig. 10. The effect on the gap width of $|U_{\bar{2}00}|$, $|U_{\bar{9}1\bar{1}}|$ and thickness.

☐ U$_{200}$, 1500 Å   + U$_{200}$, 2000 Å   ◊ U$_{911}$, 2000 Å

Fig. 11 shows a calculation of the $\bar{2}00$ disc for $Al_xGa_{1-x}As$ as a function of x. As can be seen, the intensity in the $\bar{2}00$ disc changes quite a lot as x increases. Going from pure GaAs to pure AlAs corresponds roughly to a factor of ten in the magnitude of U_{200}. In agreement with what we observed in Fig. 3, this means that the central feature in the $\bar{2}00$ disc, the black cross, gradually disappears and a white/black cross emerges. Although not shown here, this also means that the difference between the 200 disc and the $\bar{2}00$ disc almost disappears, as also was demonstrated in Fig. 3 when the magnitude of U_{200} increased. It should be noted in this connection that the reason that the patterns in Fig. 3(c) and the one for pure AlAs in Fig. 11 are not equal is that in the latter case the structure factors of all the reflections involved are changed and, owing to the dynamical interactions, this also affects the $\bar{2}00$ intensity. The fact that the black cross and thus the $\bar{2}00$ gap disappears at large Al fractions also demonstrates that the use the $\bar{2}00$ gap as a measure of x only has meaning for relative small x values, *i.e.* $x \le 0.3$–0.4.

However, as mentioned above, if we consider the whole disc, the intensity variations with Al content x are quite pronounced. Fig. 12 shows rocking curves across the $\bar{2}00$ disc as a function of different x values in $Al_xGa_{1-x}As$. These curves show quite strong variations with x, which suggests that a least-squares fitting between calculated and experimental line scans with x as the refinable parameter should have potential for giving a quite accurate value for x. Zuo, Spence & O'Keeffe (1988) have in a previous study of bonding

in GaAs shown that low-order structure factors can be measured by such a method with an accuracy well below 1%. A corresponding accuracy should therefore also be achievable for x. The accuracy, however, may be limited by several factors, *e.g.* lattice strain, lack of accurate Debye–Waller factors and/or by proper methods to remove the diffuse background due to inelastic scattering, which is generally not included in the calculations. The latter problem may be eliminated to a large extent by the use of energy filtering, which removes all inelastic scattering with energy losses above some eV (*e.g.* Mayer, Spence, Ernst & Mobus, 1991; Gubbens & Krivanek, 1993; Holmestad, Krivanek, Høier, Marthinsen & Spence, 1993).

6. Conclusions

The present study has shown that it is possible to detect the asymmetry of both GaAs and InP by the method of Taftø & Spence (1982), with carefully chosen diffraction conditions. The structure-factor magnitudes should be of the same size and the three-phase invariants involved be as close as possible to $\pm\pi/2$. The same results are believed to be valid also for other III–V semiconductors under these conditions. It is further shown that the polarity in III–IV semiconductors is determined from simple qualitative arguments. Simulations showed that the asymmetry effects that are the basis for the polarity determination for small and medium thicknesses (compared with the actual extinction lengths) are relatively independent of the specimen thickness.
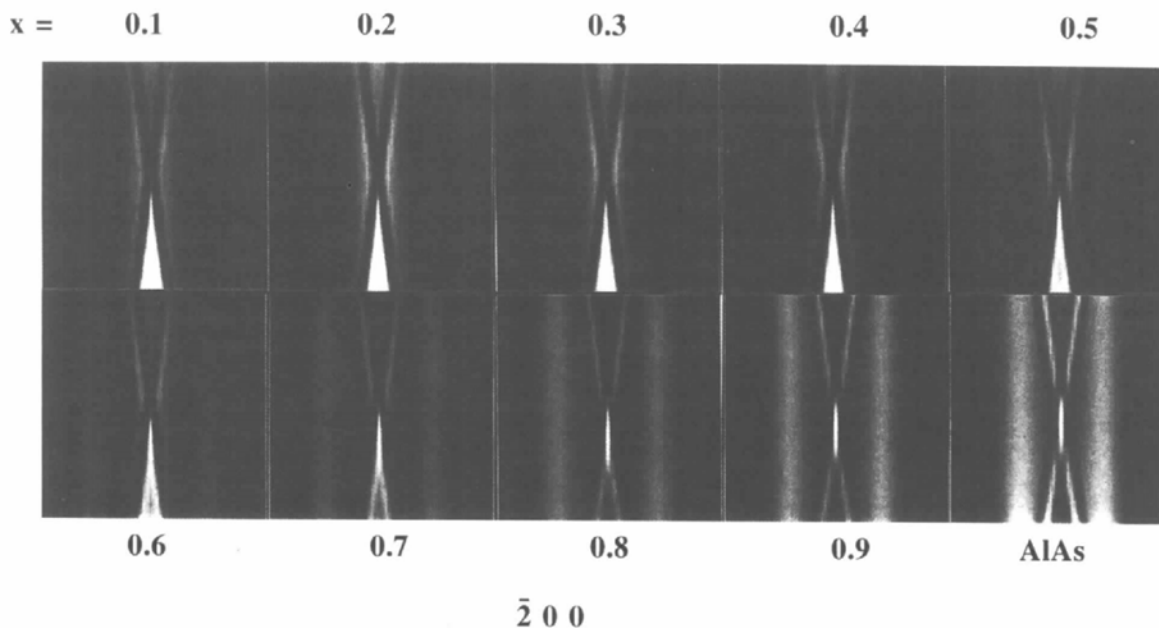

Fig. 11. Simulation of the $\bar{2}00$ reflection as a function of the Al content x in $Al_xGa_{1-x}As$. 100 keV, 2000 Å.

The gap observed in the 200 disc for GaAs was shown to be a genuine four-beam effect. It cannot be explained from three-beam calculations based on Bloch waves; however, with the assumption of the coherent multiple scattering in the four-beam case, the occurrence of a gap in only one of the conjugate discs is predicted. Furthermore, the gap width was found to depend on the different structure factors involved as well as the specimen thickness. Nevertheless, it should be possible to determine one structural parameter when knowing or carefully controlling the others by quantitatively comparing experimental and calculated rocking curves.

U_{200} of GaAs (sensitive to bonding) may be determined from the gap between the black lines in the $\overline{2}00$ disc if the other parameters can be controlled. However, U_{200} is probably equally well determined from the strong variations in ± 200 intensity oscillations itself using recently developed quantitative CBED methods (Spence, 1993).

Intensity

Fig. 12. Rocking curves for the $\overline{2}00$ reflection as a function of Al content x in $Al_xGa_{1-x}As$. 100 keV, 2000 Å.

References

Bethe, H. A. (1928). *Ann. Phys. (Leipzig),* **87,** 55–129.
Bird, D. M. (1990). *Acta Cryst.* A**46,** 208–214.
Bird, D. M. & King, Q. A. (1990). *Acta Cryst.* A**46,** 202–208.
Cowley, J. M. & Moodie, A. F. (1962). *J. Phys. Soc. Jpn,* **17,** B-II, 86–91.
Doyle, P. A. & Turner, P. S. (1968). *Acta Cryst.* A**24,** 390–397.
Eaglesham, D. J. & Humphreys, C. J. (1986). Proceedings of the XIth International Congress on Electron Microscopy, Kyoto, Japan, Vol. 1, pp. 209–210.
Gubbens, A. J. & Krivanek O. L. (1993). *Ultramicroscopy,* **51,** 146–159.
Høier, R., Bakken, L. N., Marthinsen, K. & Holmestad, R. (1993). *Ultramicroscopy,* **49,** 159–170.
Holmestad, R., Krivanek, O. L., Høier, R., Marthinsen, K. & Spence, J. C. H. (1993). *Ultramicroscopy,* **52,** 454–458.
Ishizuka, K. & Taftø, J. (1984). *Acta Cryst.* B**40,** 332–337.
Kakibayashi, K. & Nagata, F. (1986). Proceedings of the XIth International Congress on Electron Microscopy, Kyoto, Japan, Vol. 2, pp. 1495–1496.
McKernan, S. & Carter, B. (1990). Proceedings of the XIIth International Congress for Electron Microscopy, Seattle, USA, Vol. 2, pp. 500–501.
Marthinsen, K. (1993). *Acta Cryst.* A**49,** 324–330.
Marthinsen, K. & Høier, R. (1992). *Electron Microscopy 92,* Vol. 1, edited by A. Rios, J. M. Arias, L. Megias-Megias & A. Lopez-Galindo, pp. 189–190. University of Granada, Servicio de Publicaciones, Granada, Spain.
Mayer, J., Spence, J. C. H., Ernst, F. & Mobus, G. (1991). Proceedings of the 49th Annual Meeting of the Electron Microscopy Society of America, San Jose, USA, pp. 682–683.
Spellward, P. & James, D. (1991). *Inst. Phys. Conf. Ser.* No. 119, 375–379.
Spence, J. C. H. (1993). *Acta Cryst.* A**49,** 231–260.
Spence, J. C. H. & Zuo, J. M. (1992). *Electron Microdiffraction.* New York: Plenum Press.
Stobbs, W. M., Baxter, C. S., Bithell, E. G., Boothroyd, C. B., Ross, R. F. & Williams, E. J. (1989). *Microscopy of Semiconducting Materials 1989. Inst. Phys. Conf. Ser.* No. 100, pp. 271–280.
Taftø, J. & Spence, J. C. H. (1982). *J. Appl. Cryst.* **15,** 60–64.
Zuo, J. M., Gjønnes, K. & Spence, J. C. H. (1989). *J. Electron Microsc. Tech.* **12,** 29–55.
Zuo, J. M., Høier, R. & Spence, J. C. H. (1989). *Acta Cryst.* A**45,** 839–856.
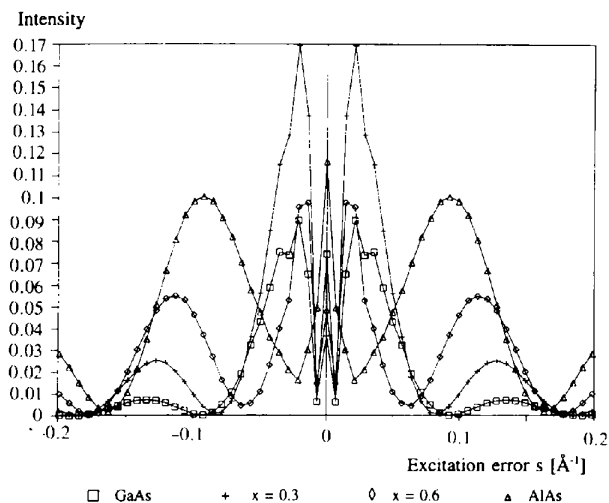Zuo, J. M., Spence, J. C. H. & O'Keeffe, M. (1988). *Phys. Rev. Lett.* **61,** 353–356.